

## Potassium Permanganate as an Oxidant for a Microfluidic Direct Formate Fuel Cell

Chunmei Liu<sup>1,\*</sup>, Haihua Liu<sup>2</sup>, Lei Liu<sup>3</sup>

<sup>1</sup> Institute of Vehicle and Transportation Engineering, Henan University of Science and Technology, Luoyang 471003, Henan Province, China

<sup>2</sup> School of Energy and Architecture, Xi'an Aeronautics University, Xi'an 710000, Shaanxi Province, China

<sup>3</sup> China Nonferrous Metals Processing Technology Co., Ltd., Luoyang 471003, Henan Province, China

\*E-mail: [liuchm800226@163.com](mailto:liuchm800226@163.com)

Received: 18 January 2019 / Accepted: 22 February 2019 / Published: 10 April 2019

---

A simple Y-type microfluidic fuel cell (MFC) was constructed with graphite plates as the electrodes. Unlike the formic acid/potassium permanganate MFCs previously reported, an alkaline sodium formate solution (a fuel) and an acid potassium permanganate solution (KMnO<sub>4</sub>, an oxidant) were adopted by our MFC. The flowing pattern in the main channel was a typical laminar flow. The effects of three parameters such as the concentrations of KMnO<sub>4</sub>, the concentrations of H<sub>2</sub>SO<sub>4</sub> (a supporting catholyte), and the flow rates of the reactants on the power output of the MFC were studied. The experimental results showed that the cell performance first improved but then decreased with increasing each parameter. The optimum MFC exhibited a maximum power density of 4.51 mW cm<sup>-2</sup> and a limiting current density of 6.67 mA cm<sup>-2</sup> with 50 mM KMnO<sub>4</sub>, 0.5 M H<sub>2</sub>SO<sub>4</sub> and a reactant flow rate of 30 mL h<sup>-1</sup>. Although the power densities and limiting current densities of our MFC are not the highest in the MFCs using KMnO<sub>4</sub> as oxidants, its open circuit voltage remains at the top. Our work demonstrates that it is feasible to construct MFCs using alkaline formate and acidic permanganate solutions, which diversifies the types of MFCs containing KMnO<sub>4</sub> as the oxidant.

---

**Keywords:** Microfluidic fuel cells; Potassium permanganate; Supporting catholyte concentration; Reactant flow rate; Open circuit voltage

### 1. INTRODUCTION

Due to the increasing power demand for modern portable electronics such as laptops, cell phones and medical instruments, micro-sized fuel cells are attracting worldwide research efforts as promising miniaturized power sources [1]. Microfluidic fuel cells (MFCs), also known as laminar flow-based fuel cells or membraneless fuel cells, have served as a major member in the family of

micro-sized fuel cells for more than a decade [2]. MFCs exploit the co-laminar flow feature of the two fluids in microscale channels to naturally separate the anolyte and catholyte without the need for high cost physical barriers such as proton exchange membranes (PEMs). This membraneless configuration can not only avoid a series of problems related to the membranes such as difficulty in water management, fuel crossover, and membrane fouling, but also gain the higher power density than the micro PEM fuel cell [3]. Thus, the development of laminar flow-based MFCs is highly desirable for making high performance and economically portable power sources.

The fuel and oxidant solutions flow laminarily in parallel with each other in a microchannel of a MFC. The supporting electrolytes in the two streams can increase electrical conductivity of the streams to promote ionic transport. The mixing of the two fluids takes place only at the liquid-liquid interface in the middle of the microchannel. In addition, the fuels, oxidants and supporting electrolytes could be optimized independently in the MFCs. The electrolytes at the anode and cathode can be both acidic or alkaline media, or different acidic/alkaline media. It is reported that MFCs with the alkaline anode solutions and the acidic cathode solutions led to a very high open circuit voltage [4].

At present, a variety of fuels have been used in MFCs such as formic acid [4-5], methanol [6], hydrogen gas [7], hydrogen peroxide [8], vanadium-based redox species [9-10] and formate [11-12]. Among these fuels, formate is proven to be an efficient and effective fuel due to its advantages including its carbon-neutral characteristic [13], high theoretical potential [14], no poisoning effect in alkaline media [15], and easy to store and transport [11].

The performance of MFCs is mainly limited by the rate of reactant transport to the active sites of the electrodes [16], especially for the cathodic half cell reactions [17]. The dissolved oxygen as an oxidant has the major limitations of limited solubility ( $2 \sim 4$  mM) in water and low diffusivity ( $\sim 2 \times 10^{-5}$  cm<sup>2</sup> s<sup>-1</sup>). If using air as the oxidant for the cathode reaction (such the cathode coined as "air-breathing cathode"), both the oxidant concentration and the diffusivity ( $\sim 0.2$  cm<sup>2</sup> s<sup>-1</sup>) can be significantly augmented. The first MFC with an air-breathing cathode was presented by Ferrigno [2]. To prevent fuel crossover and facilitate ion transport for air-breathing cathodes, blank electrolytes as supporting electrolytes are needed. However, besides the aforementioned merits of the air-breathing cathodes, some drawbacks exist. One of them is the oxygen reduction at the cathode that demands expensive noble metals (*e.g.* Pt) as catalysts.

Instead of using air as the oxidant, the performance of MFCs can also be improved with other liquid oxidants such as H<sub>2</sub>O<sub>2</sub> [18], NaClO<sub>4</sub> [19], vanadium redox species [20-21] and KMnO<sub>4</sub> [22-25]. In the presence of Pt catalyst, H<sub>2</sub>O<sub>2</sub> and NaClO<sub>4</sub> can self-decompose to release oxygen gas and chlorine gas. These bubbles could interrupt the liquid-liquid interface or the laminar flow between the two streams, leading to severe mixing of the two streams and significantly reducing the cell performance. Vanadium redox species generate no gaseous products when undergoing redox reactions and their reactions do not need catalysts, but vanadium element is toxic and must be strictly prevented from leaking. Considering the trend of miniaturization and integration for future MFCs, an ideal oxidant needs to equip with a high electrochemical activity, large solubility, no gases production during a redox reaction and environmental friendliness.

Potassium permanganate (KMnO<sub>4</sub>) is one possible candidate oxidant. It has many advantages such as a high oxidation ability, large redox potential and the proceeding of its reduction reaction with

no catalyst. Previous researches using  $\text{KMnO}_4$  as the oxidant for MFCs mainly investigated the different cell constructions such as the radial flowing of the two streams [22], the three inlets [23], and a bridge-shaped microchannel cross-section [24], or with electrospun CNx nanofibers as the cathode [25].

Unlike other researches adopting  $\text{KMnO}_4$  as the oxidant in acidic electrolytes of the MFCs [22-25, 26], the MFC in this study involves the alkaline sodium formate solution and the acidic  $\text{KMnO}_4$  solution as the fuel and oxidant, respectively. The usage of the mixed supporting electrolyte in this experiment is to promote the electrochemical reactions on the electrodes and obtain a high open circuit voltage. In this study, the effects of the oxidant concentrations, the supporting catholyte concentrations and flowing rates on the MFC performance are investigated.

## 2. EXPERIMENTAL CONSTRUCTION AND METHODS

### 2.1 MFC construction

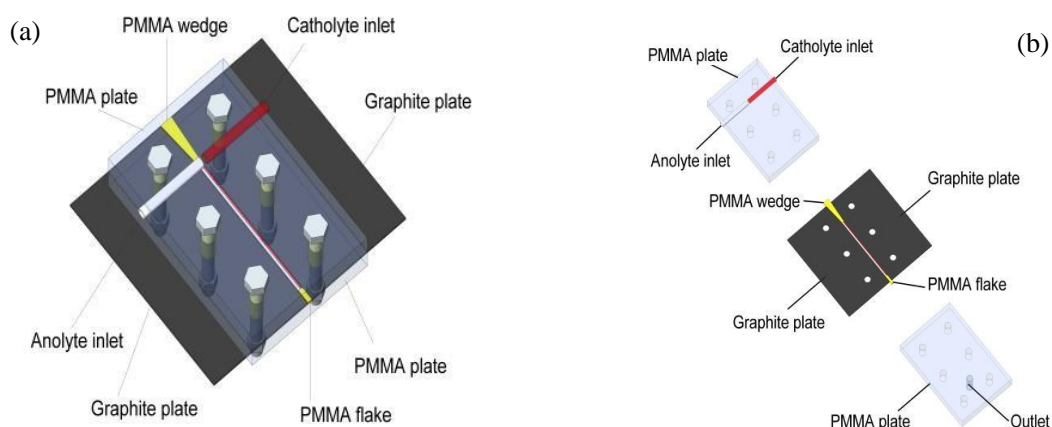


**Figure 1.** Schematic of the microfluidic fuel cell using graphite plates as electrodes ((a) the assembled MFC, (b) exploded view of the MFC. Note: The wedge and flake are made of PMMA. Here, the two plates are shown in yellow just to make them clear.).

In this experiment, a Y-shaped MFC was constructed, as schematically shown in Figure 1. The actual picture of the MFC is attached to the manuscript as Figure S1 of the Supporting Materials. The cell was comprised of two PMMA (poly methyl methacrylate) plates and two 1 mm thick graphite plates as the electrodes. The microchannel of the MFC was lined by the sides of the two graphite plates placed in parallel, with the dimensions of  $40 \text{ mm} \times 2 \text{ mm} \times 1 \text{ mm}$ . The two small PMMA plates were put at the two ends of the microchannel to separate the electrodes and seal this channel. The effective surface area of the electrode was  $0.4 \text{ cm}^2$  ( $40 \text{ mm} \times 1 \text{ mm}$ ) [27, 28]. Two 2 mm inlets were at the two sides of the top plate and proceed to connect the microchannel, while one 3 mm outlet was mounted at the bottom of the bottom plate. The whole device was eventually assembled by six 4 mm screw bolts.

Pd particles serving as anode catalysts were loaded onto the one side of the anode electrode. The Pd plating solution is 1.0 wt. %  $\text{PdCl}_2$  in 1 M HCl solution. The electrodeposition of the Pd catalyst involved a first of applying a potential of 0.0 V *vs.* Ag/AgCl reference electrode (0.198 V *vs.* standard hydrogen electrode, SHE) for 5 minutes, followed by immersing in the 5% Nafion solution

for 5 minutes. This process was repeated for five times, until the Pd catalyst loading was  $5 \text{ mg cm}^{-2}$  [28, 29]. The electrodeposition was carried out by a Zennium electrochemical workstation (Zahner, Germany) via a three electrode mode, with the graphite plate as the working electrode, an Ag/AgCl electrode in saturated KCl solution as the reference electrode, and a Pt sheet ( $10 \text{ mm} \times 50 \text{ mm} \times 0.2 \text{ mm}$ ) as the counter electrode.

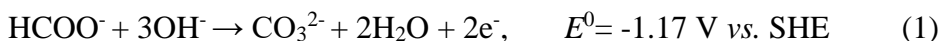
## 2.2 The visual experiment for the laminar flowing

The visual experiment for the in-parallel laminar flow of the two streams in the microchannel was recorded by Nikon D7000 (Japan) camera equipped with an AFS micro Nikon 105 mm optical lens.

## 2.3 Performance evaluation

The fuel and oxidant solution were delivered into the microchannel of the cell by a dual pass injection syringe pump (LSP02-1B, Baoding Longer Precision Pump Co., Ltd., China). The fuel solution was a mixture of 2 M sodium formate (HCOONa) and 2 M NaOH solution blended in a 1:1 volume ratio. The oxidant stream was composed of different concentrations of the  $\text{KMnO}_4$  solution as the oxidant and  $\text{H}_2\text{SO}_4$  solution as the supporting electrolyte. The cell performance was gained by a chronoamperometry method using an electrochemical workstation (Zahner, Germany). The cell voltages were varied from the open circuit to the short circuit with a decreasing potential step of 200 mV. Each cell voltage was kept for 3 minutes. The currents were recorded at the end of each potential step. The electrode potentials were the potential difference between the each electrode and the Ag/AgCl reference electrode located near the outlet. The schematic figure of experimental measurement system is shown as Figure S2 of the Supporting Material. The current density and power density were normalized to the effective electrode surface area ( $0.4 \text{ cm}^2$ ).

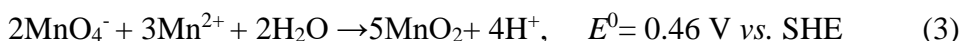
The electrochemical reaction at the anode is:



There are different routes for the cathode reaction of  $\text{KMnO}_4$  reduction, the main reduction route in acidic media is:



The generated Mn(II) ions can be oxidized by  $\text{MnO}_4^-$  in acidic solutions, producing insoluble  $\text{MnO}_2$  [30]:



The theoretical open circuit voltage (OCV) of this MFC is 2.677 V (assuming the fuel and the oxidant are completely oxidized and reduced, respectively).

### 3. RESULTS AND DISCUSSION

#### 3.1 Visual experiment of the parallel flowing

MFCs exploit the feature of two streams in a laminar flowing in a microchannel. Therefore, the laminar flow of the two streams is a prerequisite for the normal operation of MFCs. The Reynold number ( $R_e$ ) is a characteristic value to judge the flowing state, which is calculated according to the formula below [31]:

$$R_e = vD_e/\mu$$

where  $v$  is the average velocity of flow on the transversal surface of the microchannel ( $\text{m s}^{-1}$ ),  $D_e$  is the equivalent diameter (m),  $D_e = 4A/X$  [ $A$  transversal surface area of the main channel ( $\text{m}^2$ ) and  $X$  wetted perimeter (m)],  $\mu$  is the dynamic viscosity coefficient of the solution ( $\text{m}^2 \text{s}^{-1}$ ), here  $\mu$  is approximately treated as the viscosity coefficient of water at 25 °C ( $\mu = 0.871 \times 10^{-6} \text{ m}^2 \text{ s}^{-1}$  [31]). The calculated  $R_e$  values under the different flow rates are listed in Table 1. Since all  $R_e$  values are below 6, the flowing state in the microchannel is typically laminar.

**Table 1.**  $R_e$  values under the different flow rates

Flux ( $\text{mL h}^{-1}$ )	10	20	30	40
$R_e$	1.27	2.54	3.80	5.07

To further verify the laminar flow state of the two streams in the microchannel, the visual experiment was carried out. To clearly visualize the flowing state, deionized water and deionized water dyed with red ink were adopted as the two streams, respectively. In the reactor comprised of the two graphite plates without the Pd catalysts, the two fluids were simultaneously sent into the reactor by a syringe pump. The photographs of the visual experiment are shown in Figure 2. The two water streams in the main channel under various flow rates ranging from 10  $\text{mL h}^{-1}$  to 40  $\text{mL h}^{-1}$  do not mix with each other, which is consistent with the calculated  $R_e$  values.

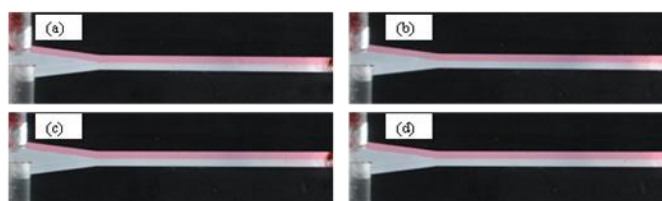


**Figure 2.** Digital photos showing the two fluids in the microchannel under different flow rates: ((a) 10  $\text{mL h}^{-1}$ , (b) 20  $\text{mL h}^{-1}$ , (c) 30  $\text{mL h}^{-1}$ , (d) 40  $\text{mL h}^{-1}$ ).

#### 3.2 Effects of $\text{KMnO}_4$ concentrations on the cell performance

$\text{KMnO}_4$  as an oxidant in our MFC plays an important role in determining the cell performance. The effects of  $\text{KMnO}_4$  concentrations ranged from 12.5 mM to 100 mM on the cell performance and electrode potentials are shown in Figure 3 and Figure 4, respectively (the flow rate is kept constant at

20 mL h<sup>-1</sup> and the H<sub>2</sub>SO<sub>4</sub> solution concentration is 0.5 M). Table 2 enlists the OCVs, the peak power densities and the limiting current densities of the MFC under the different KMnO<sub>4</sub> concentrations.

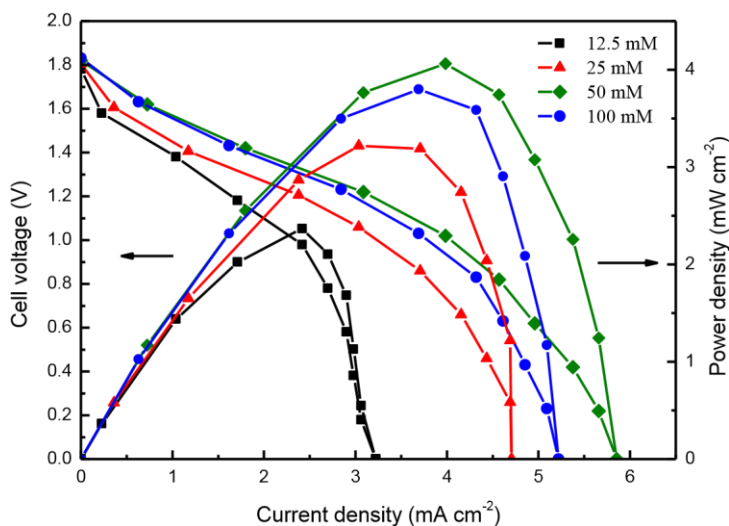


**Figure 3.** Polarization curves (left Y-axis) and power density curves (right Y-axis) at various KMnO<sub>4</sub> concentrations with 0.5 M H<sub>2</sub>SO<sub>4</sub> as a supporting electrolyte under a flow rate of 20 mL h<sup>-1</sup>.

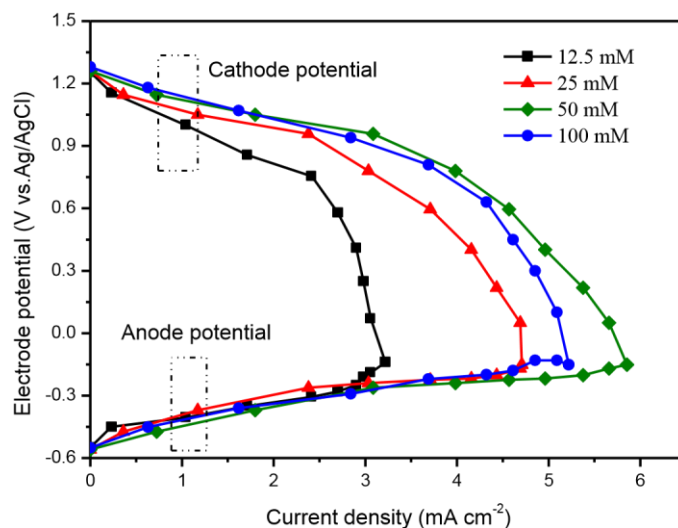


**Figure 4.** Electrode potential curves at different KMnO<sub>4</sub> concentrations containing 0.5 M H<sub>2</sub>SO<sub>4</sub> as a supporting electrolyte under a flow rate of 20 mL h<sup>-1</sup>.

Based on the results of Figure 3 and Table 2, the OCVs of the MFCs are all more than 1.78 V with different KMnO<sub>4</sub> concentrations. These OCVs are less than the theoretical cell voltage (2.677 V), which can be attributed to the two reasons. The first one is the mixing between the fuel and oxidant solutions at the intersection of the two fluids happened. The second one is existence of side reaction of (3) that results in MnO<sub>2</sub>. Nevertheless, these OCVs in the mixed media are higher than those (about 1.45 V) of the MFCs with all acidic media reported previously [31].

**Table 2.** OCVs, peak power densities and limiting current densities under the different  $\text{KMnO}_4$  concentrations

$\text{KMnO}_4$ concentrations (mM)	OCV (V)	Peak power Densities ( $\text{mW cm}^{-2}$ )	Limiting current densities ( $\text{mA cm}^{-2}$ )
12.5	1.78	2.37	3.22
25	1.81	3.22	4.71
50	1.82	4.06	5.85
100	1.83	3.80	5.22

Figure 3 illustrates that the cell performance first increases and then decreases with increasing the oxidant concentrations. When the  $\text{KMnO}_4$  concentration increases from 12.5 mM to 50 mM, the peak power density rises from  $2.37 \text{ mW cm}^{-2}$  to  $4.06 \text{ mW cm}^{-2}$  by 71.31%. This result can be ascribed to the higher oxidant concentration that not only supplies more oxidants, but also improves the transport of the oxidant to the cathode electrode. The latter promotes the electrochemical reaction rate on the cathode and improves the overall cell performance. While the oxidant concentration is further increased to 100 mM, the cell performance starts to decrease. The maximum power density and the maximal limiting current density is  $3.80 \text{ mW cm}^{-2}$  and  $5.22 \text{ mA cm}^{-2}$  at 100 mM  $\text{KMnO}_4$ , respectively. Although the higher oxidant concentration improves the oxidant ability and decreases the cathode resistance as discussed before, the more insoluble  $\text{MnO}_2$  are inevitably produced from the direct reaction of  $\text{KMnO}_4$  and  $\text{HCOONa}$  in the inner diffusion zone and from the secondary reaction of  $\text{KMnO}_4$  reduction. The yielded  $\text{MnO}_2$  could clog the microchannel and prevent the oxidant from contacting with the cathode. This negative impact exacerbates under highly concentrated  $\text{KMnO}_4$  solutions and long term operation of the MFC.

From the electrode potential plots shown in Figure 4, the cathode performance shows an obvious mass transfer limitation at 12.5 mM  $\text{KMnO}_4$ , where the cathode potential decreases sharply. When the  $\text{KMnO}_4$  concentration increases to 50 mM, the higher oxidant concentration improves the mass transfer of the oxidant and facilitates the mass transfer at the cathode. At 50 mM  $\text{KMnO}_4$ , the cell performance reaches the best. When further increasing the  $\text{KMnO}_4$  concentration to 100 mM, the cathode potential reduces slightly and the anode potential slightly increases, compared to the potentials at 50 mM  $\text{KMnO}_4$ . This phenomenon is due to the production of insoluble  $\text{MnO}_2$  that clogs the microchannel and hinders mass transfer of the reactants.

### 3.3 Effects of $\text{H}_2\text{SO}_4$ concentrations on the cell performance

$\text{H}_2\text{SO}_4$  as the supporting electrolyte in the catholyte provides the  $\text{H}^+$  ions that not only improve the electrical conductivity of the catholyte, but also promote the oxidation activity of  $\text{KMnO}_4$ .

The effects of  $\text{H}_2\text{SO}_4$  concentrations (0.25, 0.5, 1.0 M) on the cell performance and electrode potentials are illustrated in Figure 5 and Figure 6, respectively (the flow rate is kept constant at  $20 \text{ mL h}^{-1}$  and the concentration of  $\text{KMnO}_4$  is 50 mM). And the OCVs, the peak power densities and the limiting current densities of the MFC under different  $\text{H}_2\text{SO}_4$  concentrations are summarized in Table 3.

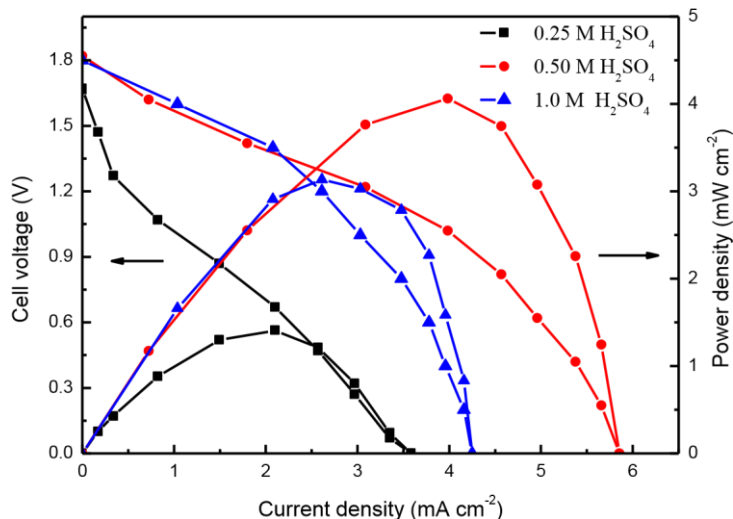


**Figure 5.** Polarization curves (left Y-axis) and power density curves (right Y-axis) at different H<sub>2</sub>SO<sub>4</sub> concentrations of 50 mM KMnO<sub>4</sub> and a flow rate of 20 mL h<sup>-1</sup>.

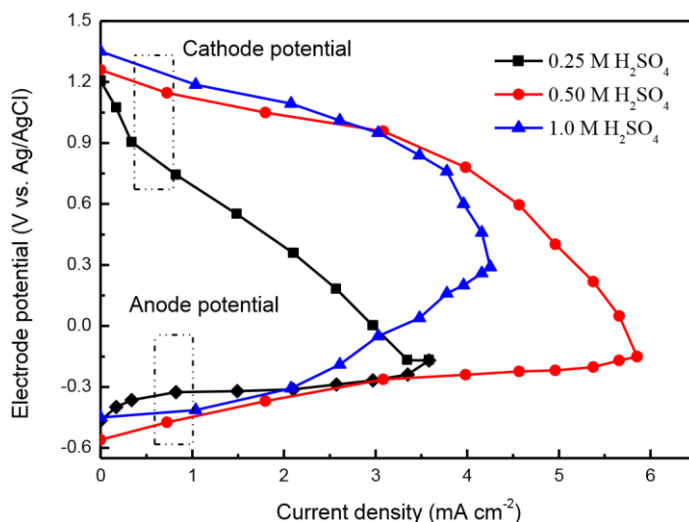


**Figure 6.** Electrode potential curves under different H<sub>2</sub>SO<sub>4</sub> concentrations at 50 mM KMnO<sub>4</sub> and a flow rate of 20 mL h<sup>-1</sup>.

**Table 3.** OCVs, peak power densities and limiting current densities under the different H<sub>2</sub>SO<sub>4</sub> concentrations

H <sub>2</sub> SO <sub>4</sub> concentrations (M)	OCV (V)	Peak power Densities (mW cm <sup>-2</sup> )	Limiting current densities (mA cm <sup>-2</sup> )
0.25	1.67	1.41	3.58
0.5	1.82	4.06	5.85
1.0	1.80	3.13	4.25

Concluded from Figure 5 and Table 3, the peak power density and the limiting current density of the cell with 0.5 M H<sub>2</sub>SO<sub>4</sub> is 4.06 mW cm<sup>-2</sup> and 5.85 mA cm<sup>-2</sup>, respectively, increasing by 1.87

times and 0.96 times than those of the MFCs with 0.25 M H<sub>2</sub>SO<sub>4</sub>. The enhancement is due to the increased supporting electrolyte concentration that accelerates the mass transfer of cathode reactions and reduces the ohmic resistance at the cathode. In addition, the reduction of KMnO<sub>4</sub> at the cathode is aided by H<sup>+</sup> and enhanced with the augment of H<sup>+</sup> concentrations. If the supporting electrolyte concentration is low, the H<sup>+</sup> concentration near the cathode surface is small, leading to slow transfer rate of H<sup>+</sup> to the cathode electrode and compromising cell performance. At 1.0 M H<sub>2</sub>SO<sub>4</sub>, the cell performance decreases appreciably at the intermediate and high current densities, except that the cell performance is a little higher than that of cell at 0.5 M H<sub>2</sub>SO<sub>4</sub> at the low current density (< 2.08 mA cm<sup>-2</sup>). This phenomenon could be explained by the poisoning effect of SO<sub>4</sub><sup>2-</sup> on the catalyst activity of Pd catalysts [32]. Degradation in the catalytic activity could increase the anode potential to the positive values, deteriorating the anode performance thus decreasing the cell performance.

### 3.4 Effects of flow rates on the cell performance

The flow rate is one of the key factors dictating the cell performance by influencing the flowing state and the mass transfer of the reactants and products. The effects of flow rates from 10 mL h<sup>-1</sup> to 40 mL h<sup>-1</sup> on the cell performance and electrode potentials are investigated, with results presented in Figure 7 and Figure 8, respectively (the concentrations of KMnO<sub>4</sub> and H<sub>2</sub>SO<sub>4</sub> solutions are kept constant at 50 mM and 0.5 M, respectively). The OCVs, the peak power densities and the limiting current densities of the MFC under the different flow rates are summarized in Table 4.

From Figure 7 and Table 4, the cell performance increases with the flow rate from 10 mL h<sup>-1</sup> to 30 mL h<sup>-1</sup>. It is mainly due to the improvement in the flow rate which is feasible to not only transport the reactants to the electrodes, but also take the products out of the main channel. These improve the mass transfer and promote the electrochemical reactions on the electrodes. The peak power density and limiting current density of the MFC at a flow rate of 30 mL h<sup>-1</sup> is 4.51 mW cm<sup>-2</sup> and 6.67 mA cm<sup>-2</sup>, respectively, 2.03 times and 1.47 times higher than those of MFCs at 10 mL h<sup>-1</sup>. When the flow rate is further increased to 40 mL h<sup>-1</sup>, the cell performance decreases. This decrement is because that the further increased flow rate can cause a hydraulic instability [27-29] in the microchannel. This fluid instability destroys the liquid-liquid interface of the laminar flow and mixes the two streams. Therefore, little electricity can be gained since the oxidants and fuels react directly in the fluids rather than through the external electric circuit.

It is noted that the OCV of the cell at 10 mL h<sup>-1</sup> is about 1.65 V, lower than 1.82 V and 1.83 V at 20 mL h<sup>-1</sup> and 30 mL h<sup>-1</sup>, respectively. The reason is that the slow flow rate likely induces transverse diffusion of the two streams, as observed in previous works [33]. The OCV at 40 mL h<sup>-1</sup> is 1.76 V, less than 1.82 V at 20 mL h<sup>-1</sup>, due to the serious mixing of the fuel and oxidant streams at the high flow rate.

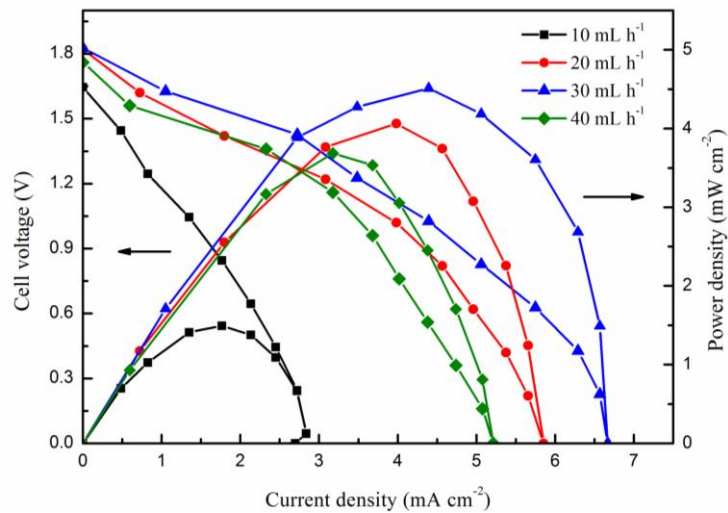


**Figure 7.** Polarization curves (left Y-axis) and power density curves (right Y-axis) at different flow rates with 50 mM  $\text{KMnO}_4$  containing 0.5 M  $\text{H}_2\text{SO}_4$  as a supporting electrolyte.

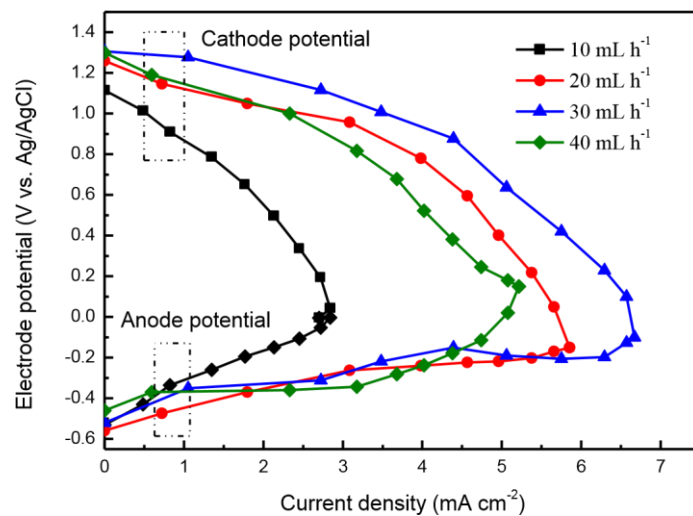


**Figure 8.** Electrode potential curves at different flow rates with 50 mM  $\text{KMnO}_4$  containing 0.5 M  $\text{H}_2\text{SO}_4$  as a supporting electrolyte.

**Table 4.** OCVs, peak power densities and limiting current densities under the different flow rates

flow rates ( $\text{mL h}^{-1}$ )	OCV (V)	Peak power Densities ( $\text{mW cm}^{-2}$ )	Limiting current densities ( $\text{mA cm}^{-2}$ )
10	1.65	1.49	2.70
20	1.82	4.06	5.85
30	1.83	4.51	6.67
40	1.76	3.69	5.22

As seen from the electrode potentials of Figure 8, at the flow rate of  $10 \text{ mL h}^{-1}$ , the cathode is under serious mass transfer limitation, because the reactants could not be supplied in time. At  $30 \text{ mL h}^{-1}$ , the cell performance is the best owing to the improvement in the mass transfer with the increase in

the flow rate. While at 40 mL h<sup>-1</sup>, the larger flow rate disturbs the laminar liquid-liquid separation interface and mixes the oxidant and the fuel, leading to considerable decrease in the cathode potentials and increase in the anode potentials.

To compare our cell performance with other reported MFCs with KMnO<sub>4</sub> as the oxidant, the peak power densities, limiting current densities of these MFCs are presented in Table 5. From Table 5, we can see that except the MFC by López-Montesinos [19], the peak power density of our MFC is the highest, suggesting the MFC with an alkaline sodium formate as the fuel and an acidic KMnO<sub>4</sub> as the oxidant is feasible for achieving a high performance. In addition, our MFC has an outstanding advantage of a simple construction and no need of cathode catalyst. In the further study to enhance our MFC performance, we can adopt other flowing patterns such as the sequential flow to improve the mass transfer in the cell.

**Table 5.** Peak power densities and limiting current densities of the MFCs with KMnO<sub>4</sub> as the oxidant

MFC	Configuration or Electrode features	Cathode Catalyst	Peak power Densities (mW cm <sup>-2</sup> )	Limiting current densities (mA cm <sup>-2</sup> )
Our	Y-type	No	4.51	6.67
Choban [26]	Y-type	Pt black	2.4	8
Sun [23]	Three inlets	Pt	0.7	2.6
Salloum [22]	Sequential flow	Pt black	2.8	5
López-Montesinos [24]	Bridged shaped	No	26	35
Jindal [25]	Electrospun CNx nanofibers as cathode	Pt and Au	3.43	9.79

#### 4. CONCLUSIONS

In this study, a Y-shaped MFC with two graphite plates as the electrodes was assembled and studied. This device had advantages such as easy to be constructed and feasible to a visual experiment for the laminar flowing in the microchannel. The microfluidic fuel cell adopted an alkaline sodium formate as the fuel and an acidic KMnO<sub>4</sub> as the oxidant. The effects of the oxidant concentrations, the supporting catholyte concentrations and the flow rates on the MFC performance were systematically investigated. Increasing the three parameters is observed to first increase but then decrease the cell performance. The optimal condition to achieve the best cell performance is determined to be 50 mM KMnO<sub>4</sub>, 0.5 M H<sub>2</sub>SO<sub>4</sub> and a flow rate of 30 mL h<sup>-1</sup>. Under these conditions, the MFC displays the maximal power density of 4.51 mW cm<sup>-2</sup> and the largest limiting current density of 6.67 mA cm<sup>-2</sup>. Further increasing the KMnO<sub>4</sub> concentration to 100 mM lowers the cell performance due to the formation of a large amount of insoluble MnO<sub>2</sub> product from reduction of KMnO<sub>4</sub> that clogs the microchannel, and hinders the mass transfer of the reactants to the electrode and the products out from the microchannel. At 1.0 M H<sub>2</sub>SO<sub>4</sub>, the cell performance declines, because more SO<sub>4</sub><sup>2-</sup> ions diffuse to the anode that poison the Pd catalyst. When the flowing rate is more than 30 mL h<sup>-1</sup>, hydraulic instability happens and destroys the laminar liquid-liquid interface, seriously mixing the two fluids and decreasing the cell performance.

In view of the insoluble  $\text{MnO}_2$  product from the reduction reaction of  $\text{KMnO}_4$ , this MFC construction might be improved by adding another inlet to introduce the third electrolyte to separate the  $\text{KMnO}_4$  solution and  $\text{HCOONa}$  solution.

#### CONFLICTS OF INTEREST

There are no conflicts to declare.

#### ACKNOWLEDGEMENTS

This work is supported by the National Natural Science Foundation of China (No.51506046).

#### SUPPORTING MATERIAL:

##### *S1 Photograph of a completed microfluidic fuel cell*

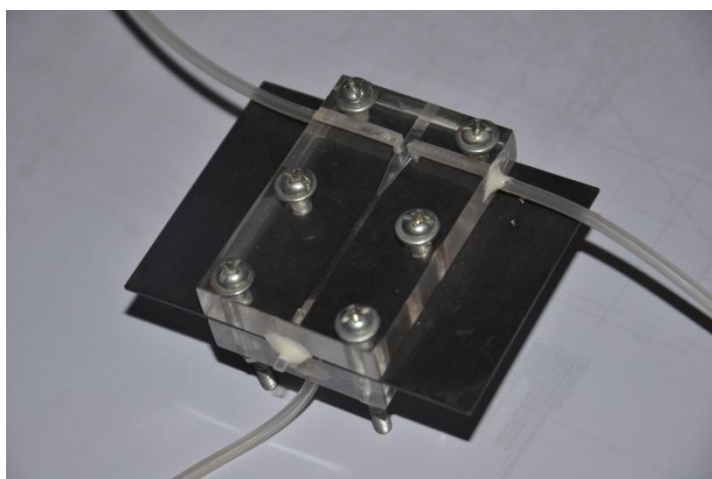


**Figure S1.** Photograph of a completed microfluidic fuel cell

Figure S1 shows the actual configuration of the Y-type MFC. The two silicone tubes and one silicone tube were glued by silica gel at the two inlets and the one outlet, respectively. The two end plates were glued on the main body of our MFC.

##### *S2 Experiment measurement system*

Figure S2 shows the schematic configuration of the Y-type MFC measurement system adopting the external reference electrode.

In this study, the polarization curves were gained by a chronoamperometry method using the electrochemical workstation (Zahner, Germany) with a two-electrode configuration. Individual anodic and cathodic potentials were obtained versus an external  $\text{Ag}/\text{AgCl}$  electrode in saturated  $\text{KCl}$  solution as the reference electrode by in situ measuring the voltage difference between the electrode and the reference electrode. The reference electrode was put near at the outlet of the MFC. This configuration

was also used in other works [27, 34]. It is worth noting that the porous ceramics at the front end of the reference electrode should be inserted into the electrolyte from the outlet of the MFC.

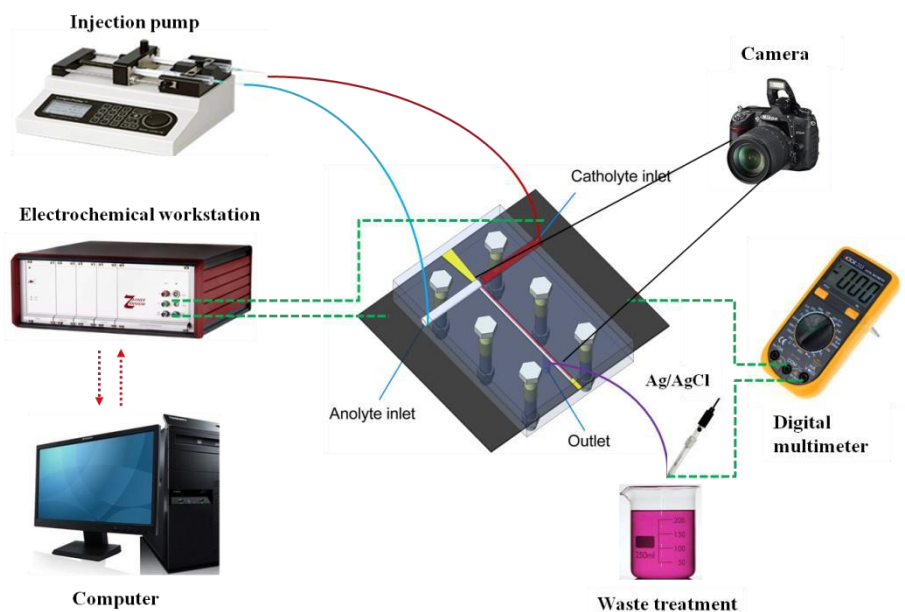


**Figure S2.** Schematic configuration of the Y-type MFC measurement system using the external reference electrode

## References

1. C. K. Dyer, *J. Power Sources*, 106 (2002) 31-34.
2. R. Ferrigno, A. D. Stroock, T. D. Clark, M. Mayer and G. M. Whitesides, *J. Am. Chem. Soc.*, 124 (2002) 12930-12931.
3. J. L. Cohen, D. A. Westly, A. Pechenik and H. D. Abruña, *J. Power Sources*, 139 (2005) 96-105.
4. N. D. Mota, D. A. Finkelstein, J. D. Kirtland, C. A. Rodriguez, A. D. Stroock and H. D. Abruña, *J. Am. Chem. Soc.*, 134 (2012) 6076-6079.
5. R. S. Jayashree, L. Gancs, E. R. Choban, A. Primak, D. Natarajan, L. J. Markoski and P. J. A. Kenis, *J. Am. Chem. Soc.*, 127 (2005) 16758-16759.
6. A. S. Hollinger, R. J. Maloney, R. S. Jayashree, D. Natarajan, L. J. Markoski and P. J. A. Kenis, *J. Power Sources*, 195 (2010) 3523-3528.
7. J. An, Y. B. Kim, J. Park, T. M. Gür and F. B. Prinz, *Nano Lett.*, 13 (2013) 4551-4555.
8. S. A. M. Shaegh, N. T. Nguyen, S. M. M. Ehteshami and S. H. Chan, *Energy Environ. Sci.*, 5 (2012) 8225-8228.
9. E. Kjeang, B. T. Proctor, A. G. Brolo, D. A. Harrington, N. Djilali and D. Sinton, *Electrochim. Acta*, 52 (2007) 4942-4946.
10. L. Li, G. Nikiforidis, M. K. H. Leung and W. A. Daoud, *Appl. Energ.*, 177 (2016) 729-739.
11. E. Kjeang, R. Michel, D. A. Harrington, D. Sinton and N. Djilali, *Electrochim. Acta*, 54 (2008) 698-705.
12. Y. S. Li, H. Wu, Y. L. He, Y. Liu and L. Jin, *J. Power Sources*, 287 (2015) 75-80.
13. X. Cheng, R. Chen, X. Zhu, Q. Liao, X. He, S. Li and L. Li, *Int. J. Hydrogen Energy*, 41 (2016) 2457-2465.
14. L. An, T. S. Zhao, S. Y. Shen, Q. X. Wu and R. Chen, *Int. J. Hydrogen Energy*, 35 (2010) 4329-4335.
15. X.W. Yu and A. Manthiram, *Appl. Catal. B Environ.*, 165 (2015) 63-67.

16. M. H. Chang, F. Chen and N. S. Fang, *J. Power Sources*, 159 (2006) 810-816.
17. E. R. Choban, P. Waszczuk, and P. J. A. Kenis, *Solid-State Lett.*, 8 (2005) A348-A352.
18. F. L. Chen, M. H. Chang and C. W. Hsu, *Electrochim. Acta*, 52 (2007) 7270-7277.
19. E. Kjeang, R. Michel, D. A. Harrington, D. Sinton and N. Djilali, *Electrochim. Acta*, 54 (2008) 698-705.
20. M.-A. Goulet, M. Skyllas-Kazacos and E. Kjeang, *Carbon*, 101 (2016) 390-398.
21. M.-A. Goulet, O.A. Ibrahim, W. H. J. Kim and E. Kjeang, *J. Power Sources*, 339 (2017) 80-85.
22. K. S. Salloum, J. R. Hayes, C. A. Friesen and J. D. Posner, *J. Power Sources*, 180 (2008) 243-252.
23. M. H. Sun, G. V. Casquillas, S. S. Guo, J. Shi, H. Ji, Q. Ouyang and Y. Chen, *Microelectron. Eng.*, 84 (2007) 1182-1185.
24. P. O. López-Montesinos, N. Yossakda, A. Schmidt, F. R. Brushett, W. E. Pelton and P. J. A. Kenis, *J. Power Sources*, 196 (2011) 4638-4645.
25. A. Jindal, S. Basu, N. Chauhan, T. Ukai, D. S. Kumar and K. T. Samudhyatha, *J. Power Sources*, 342 (2017) 165-174.
26. E. R. Choban, L. J. Markoski, A. Wieckowski and P. J. A. Kenis, *J. Power Sources*, 128 (2004) 54-60.
27. D. D. Ye, Y. Yang, J. Li, X. Zhu, Q. Liao and B. Zhang, *Biomicrofluidics*, 9 (2015) 064110-1-064110-8.
28. D. D. Ye, Y. Yang, J. Li, X. Zhu, Q. Liao, B. W. Deng and R. Chen, *Int. J. Hydrogen Energy*, 38 (2013) 15710-15715.
29. B. Zhang, D. D. Ye, J. Li, X. Zhu and Q. Liao, *J. Power Sources*, 214 (2012) 277-284.
30. F. A. Cotton and G. Wilkinson, *Advanced Inorganic Chemistry*, 4th ed., John Wiley & Sons, 1980.
31. A. Li, S. H. Chan and N.-T. Nguyen, *J. Micromech. Microeng.*, 17 (2007) 1107-1115.
32. R. S. Jayashree, M. Mitchell, D. Natarajan, L. J. Markoski and P. J. A. Kenis, *Langmuir*, 23 (2007) 6871-6874.
33. M.-A. Goulet and E. Kjeang, *Electrochim. Acta*, 140 (2014) 217-224.
34. X. Zhu, B. Zhang, D. D. Ye, J. Li and Q. Liao, *J. Power Sources*, 247 (2014) 346-353.